SANDIA REPORT
SAND2006-7678
Unlimited Release
Printed March 2007

Nano-Scale Optical and Electrical Probes of Materials and Processes

Katherine H. A. Bogart

Prepared by
Sandia National Laboratories
Albuquerque, New Mexico 87185 and Livermore, California 94550

Sandia is a multiprogram laboratory operated by Sandia Corporation,
a Lockheed Martin Company, for the United States Department of Energy's
National Nuclear Security Administration under Contract DE-AC04-94AL85000.

Issued by Sandia National Laboratories, operated for the United States Department of Energy by Sandia Corporation.

Available to DOE and DOE contractors from
U.S. Department of Energy
Office of Scientific and Technical Information
P.O. Box 62
Oak Ridge, TN 37831

Telephone: (865) 576-8401
Facsimile: (865) 576-5728
E-Mail: reports@adonis.osti.gov
Online ordering: http://www.osti.gov/bridge

Available to the public from
U.S. Department of Commerce
National Technical Information Service
5285 Port Royal Rd.
Springfield, VA 22161

Telephone: (800) 553-6847
Facsimile: (703) 605-6900
E-Mail: orders@ntis.fedworld.gov
Online order: http://www.ntis.gov/help/ordermethods.asp?loc=7-4-0#online

SAND2006-7678
Unlimited Release
Printed March 2007

Nano-Scale Optical and Electrical Probes of Materials and Processes

Katherine H. A. Bogart, Advanced Materials Science

Sandia National Laboratories
P.O. Box 5800
Albuquerque, NM 87185

Abstract

This report describes the investigations and milestones of the Nano-Scale Optical and Electrical Probes of Materials and Processes Junior/Senior LDRD. The goal of this LDRD was to improve our understanding of radiative and non-radiative mechanisms at the nanometer scale with the aim of increasing LED and solar cell efficiencies. These non-radiative mechanisms were investigated using a unique combination of optical and scanning-probe microscopy methods for surface, materials, and device evaluation. For this research we utilized our new near-field scanning optical microscope (NSOM) system to aid in understanding of defect-related emission issues for GaN-based materials. We observed micrometer-scale variations in photoluminescence (PL) intensity for GaN films grown on Cantilever Epitaxy pattern substrates, with lower PL intensity observed in regions with higher dislocation densities. By adding electrical probes to the NSOM system, the photocurrent and surface morphology could be measured concurrently. Using this capability we observed reduced emission in InGaN MQW LEDs near hillock-shaped material defects. In spatially- and spectrally-resolved PL studies, the emission intensity and measured wavelength varied across the wafer, suggesting the possibility of indium segregation within the InGaN quantum wells. Blue-shifting of the InGaN MQW wavelength due to thinning of quantum wells was also observed on top of large-scale (μm) defect structures in GaN. As a direct result of this program, we have expanded the awareness of our new NSOM/multifunctional SPM capability at Sandia and formed several collaborations within Sandia and with NINE Universities. Possible future investigations with these new collaborators might include GaN-based compound semiconductors for green LEDs, nanoscale materials science, and nanostructures, novel application of polymers for OLEDs, and phase imprint lithography for large area 3D nanostructures.

Acknowledgements

The author would like to acknowledge the following colleagues for their important contributions to this work:

Mary H. Crawford, Semiconductor Materials and Device Sciences (1123), for tremendous support, help, and mentoring in her position as Senior/Mentor for this LDRD program.

Team Members Cy H. Fujimoto, Fuels and Energy Transitions (6338), and Michael A. Quintana, Solar Technologies (6337) for their interest and contributions to bringing up a new analysis capability.

Jeff Nelson, Solar Technologies, (6337), for assistance in accommodating changes to resources.

Steven R. Kurtz, Semiconductor Materials and Device Sciences (1123), for his interest, energy, and drive to bring up the NSOM system and starting our research into nano-scale, concurrent optical, electrical, and morphological studies of GaN-based materials for lighting. Steve passed away during this program and his is still missed not only for his expertise in compound semiconductor physics, but also for his unique and strong personality.

Contents

Figures

Executive Summary

This report describes the investigations and milestones of the Nano-Scale Optical and Electrical Probes of Materials and Processes Junior/Senior LDRD. The goal of this LDRD was to improve our understanding of radiative and non-radiative mechanisms at the nanometer scale with the aim of increasing LED and solar cell efficiencies. These non-radiative mechanisms were investigated using a unique combination of optical and scanning-probe microscopy methods for surface, materials, and device evaluation. For this research we utilized our new near-field scanning optical microscope (NSOM) system to aid in understanding of defect-related emission issues for GaN-based materials. We observed micrometer-scale variations in photoluminescence (PL) intensity for GaN films grown on Cantilever Epitaxy pattern substrates, with lower PL intensity observed in regions with higher dislocation densities. By adding electrical probes to the NSOM system, the photocurrent and surface morphology could be measured concurrently. Using this capability we observed reduced emission in InGaN MQW LEDs near hillock-shaped material defects. In spatially- and spectrally-resolved PL studies, the emission intensity and measured wavelength varied across the wafer, suggesting the possibility of indium segregation within the InGaN quantum wells. Blue-shifting of the InGaN MQW wavelength due to thinning of quantum wells was also observed on top of large-scale (μm) defect structures in GaN. As a direct result of this program, we have expanded the awareness of our new NSOM/multifunctional SPM capability at Sandia and formed several collaborations within Sandia and with NINE Universities. Possible future investigations with these new collaborators might include GaN-based compound semiconductors for green LEDs, nanoscale materials science, and nanostructures, novel application of polymers for OLEDs, and phase imprint lithography for large area 3D nanostructures.

Introduction

Solid State Lighting (SSL) is the second semiconductor revolution. In SSL, solid compound semiconductor-based light emitting diodes (LEDs) replace gaseous incandescent and fluorescent bulbs. LEDs are compact, shock resistant, have long lifetimes (100,000 hours), and can be integrated into complex lighting control systems. Most importantly, implementation of LEDs in SSL is expected to have a tremendous impact on global energy savings due to the higher energy efficiencies in light production. An overall SSL goal of 50% efficiency by 2025 has been set by the Department of Energy and efficiency increases of ~10x for incandescent and ~2x for fluorescent are expected. Some lasers and LEDs have already achieved ~50% efficiency in the infra-red, and current research funding is being directed to achieve similar results at all visible wavelengths. Approximately 20% of all electric energy consumption is used for general purpose illumination and if the efficiency of these solid state sources is increased to the desired levels a decrease in total electricity consumption of 10% is expected by 2025.

Both organic and inorganic materials are currently being developed to produce solid state lighting. In our group at Sandia, we have focused on inorganic light emitters based on group III-V compound semiconductors. To date bright red emitters have been fabricated using the AlInGaP family of alloys and blue and green emitters have been fabricated using the AlInGaN family of alloys. One major drawback of the group III nitrides is the lack of lattice-matched substrates for growth. Typically, GaN is grown on sapphire, resulting in high levels of dislocations and other defects which contribute to reduced device efficiencies. In addition disparate growth temperatures are required for indium incorporation into the InGaN which results in material inhomogeneities, point defect generation, and impurity incorporation; all of which may produce possible non-radiative recombination centers and limit luminescent efficiency. The specific effect of these imperfections on the optical and electrical properties of GaN-based materials is not well understood. The production of InGaN–based LEDs is also hampered by non-linear growth phenomena, resulting in poor control and stability of MOCVD systems. Despite the high level of dislocations, the InGaN-based LEDs are surprisingly bright due to the wide band gap, the high exciton binding energy, and the potential localization of electrons and holes away from dislocation cores in the multiple quantum wells.

For InGaN, one specific material inhomogeneity involves In-rich regions formed by phase separation in InGaN, with optical emission occurring preferentially in these regions. Concurrent optical, electrical, and morphological measurements of these imperfections are limited by instrument incompatibilities and by the sub-micrometer size of these features. In addition, UV-NSOM systems ($\leq$ 325 nm) for nitride research are relatively new. There have been few previous NSOM studies of InGaN alloys with widely varying results. Several groups have reported variations in PL intensities and wavelengths near defects in epitaxial InGaN, demonstrating the inhomogeneous nature of these materials.[1,2] However below 100 nm the detection of In-rich clusters by NSOM-PL is not as clear. Jeong observed high efficiency macroscopic PL intensities in areas with spatially inhomogeneous luminescence intensities, suggesting localization of excitons in In-rich quantum dot-like structures and non-radiative recombination centers.[3] Vertikov, et al., observed no variation in PL wavelength (due to In concentration variation) with 100 nm resolution,[2] but suggested In cluster sizes may average 50 nm with a large size

dispersion and therefore not detectable with 100 nm resolution.[4] Kim, *et al.*, observed spatial variations in the luminescence wavelength which indicate that composition fluctuations are enhanced with increasing In in the film, but suggested that the regions of high intensity are not due to a localized clustering of the indium.[5] In general, these studies all observed spatial PL intensity and wavelength variations in InGaN alloys, however no definitive proof of indium-segregation has been presented. Additionally, no studies have been conducted where the materials are characterized well enough to determine the extent of indium-segregation on the dislocation density or growth conditions.

Until recently, UV capable, near-field scanning optical microscopy (NSOM) and electrical scanning-probe microscopies (SPM) with nanometer-resolution have not been available, in-house, to contribute to Sandia's semiconductor material and device research. Our dedicated instrument has the capability to perform high-resolution (100 nm) NSOM and SPM measurements concurrently, as well as lower resolution (~ 1 μm) optical confocal measurements. Our instrument is unique since the optics extends the available wavelength range into the UV (≥ 325 nm) and the Al-coated Si/Si_3N_4 AFM probe tips provide more robust NSOM apertures (see Instrument Description for more details).

With this Junior/Senior LDRD, we are supporting research programs by applying this novel tool to energy conversion device technologies, specifically III-nitride-based LEDs, II-VI-based solar cells, and organics LEDs (OLEDs). The current scope of our work includes creating confocal- and NSOM-based, spectrally-resolved photoluminescence (PL) spatial images of blue and green InGaN quantum wells (QWs), resolving spatially (≤1 μm confocal and ≤ 100 nm NSOM) regions of indium segregation in InGaN QWs, and comparing photocurrent and morphological images of LEDs to identify dislocations and other features. The initial research focused on identifying if indium segregation occurs in InGaN-based materials and characterizing if the optical and electrical inhomogeneities in the InGaN-based structures were correlated to growth morphology. Incorporation of up to ~ 10 % indium into InGaN QWs increases the radiative efficiency of LEDs and lasers however as the indium percentage is increased beyond 10 % the radiative efficiency decreases. Also, as indium is added to the InGaN, the optical emission occurs at longer than expected wavelengths compared to bulk InGaN emission for the same indium concentration. Two theories have been proposed as to explain the red-shifting emission in InGaN QWs. First, it was initially believed that the red-shift in emission occurs because electrons and holes are preferentially trapped in the indium-rich regions formed by phase separation, which would lead a red-shift of the emission. More recently, however, the strong piezoelectric forces on the QWs distort the band-structure and lead to red-shifting of the QW emission. While experimental evidence exists for both models, the difference in materials studied makes any attempt to prove or disprove either theory difficult.

Our initial NSOM experiments have revealed highly inhomogeneous emission from domains in InGaN alloys in QWs. In Fig. 1, the NSOM peak photoluminescence wavelength is shown where the color purple indicates indium deficient regions and the color yellow indicates indium rich regions. We believe the data in Figure 1 may be the first reported NSOM observation of indium segregation.

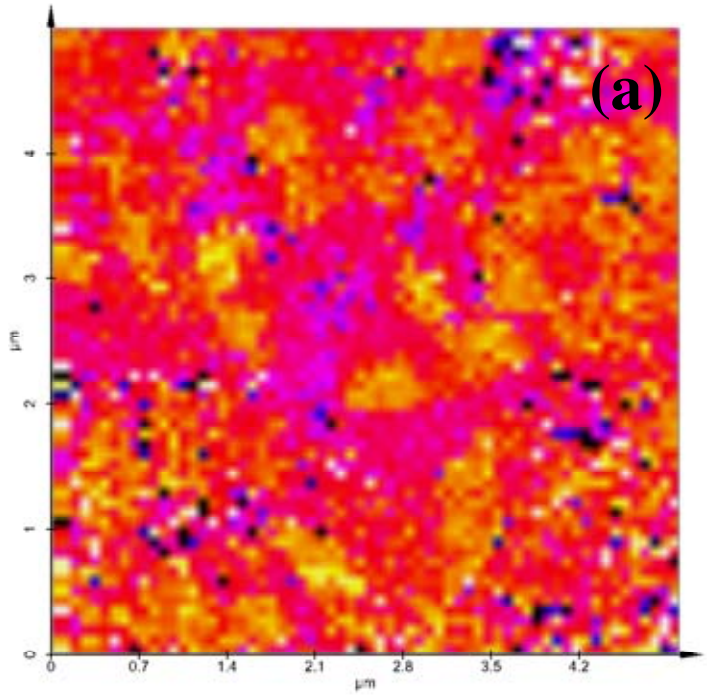

Fig. 1. NSOM photoluminescence image (4.5 x 4.5 µm) of an InGaN single quantum well. The variability in indium composition is shown as a function of peak wavelength where purple (392 nm) indicates In-poor and yellow (396 nm) indicates In-rich phases.

In future work, the position of emission domains will be compared with topography, and the location of dislocations will be detected with (AFM). The size and density of the In-rich regions will be characterized for different growth conditions and post-growth annealing procedures. Trends in InGaN growth, nano-structure, and emission intensity will be correlated in order to optimize radiative efficiency and LED performance.

For II-VI material solar cells, comparisons of high-resolution photo-current and morphological images of LEDs and solar cells will be made to identify dislocations and other features which affect minority carrier lifetime.

For OLEDs, our planned work includes macro-, micro-, and nano-scale PL of organic polymers. With combined optical and scanning probe microscopies, we hope to improve our understanding of non-radiative mechanisms within nanostructures and ultimately increase energy efficiencies of LED and solar cell devices. The benefit of performing this work in this LDRD is that the semiconductor materials will be better controlled since they are grown at Sandia, and numerous experimental techniques will be applied to understand the bulk nature of these samples. In addition, specific problems can be studied from a series of samples where a specific growth parameter is varied systematically.

Goals and Milestones

The goal of this LDRD was to improve our understanding of the radiative and non-radiative mechanisms within nanostructures using a combination of optical and scanning-probe microscopy methods for surface, materials, and device analyses to increase LED

and solar cell efficiencies. During the first year of the LDRD, the milestones were divided into two areas, SSL Nitride LEDs and Solar Cells. For the LEDs, the milestones were 1) identify the source and extent of indium segregation in InGaN alloys, 2) identify nanostructures which enhance or decrease radiative recombination in GaN-based alloys, and 3) add electrical scanning probe microscopy (SPM) capabilities to the system. The solar cell milestones were 1) identify nanofeatures which produce "dead spots" in CdTe materials, 2) image cross-sections of II-VI/CIS solar cells and identify the location of the p-n junction, and 3) evaluate the effectiveness of textures surfaces. Our achievement of these milestones was adversely affected by unexpected medical leave by both the Junior and Senior participants, by reallocation of solar cell resources and team members, and by the untimely death of Steve Kurtz.

Mary H. Crawford was selected as the new Senior Mentor for the second year of this LDRD. The LED milestones for the second year were extensions of the same areas as the first year. Cy H. Fujimoto was added as a Team Member to replace Michael A. Quintana, in the area of organic LEDs. New milestones were determined for the OLEDs 1) obtain macro- and micro-scale PL from OLED polymeric materials, and for the NSOM system 1) upgrade operating software and CCD collection optics and 2) expand awareness of NSOM capabilities and form new collaborations at Sandia. During the second year, we determined that the UV optics train had degraded. Replacement of the UV optics took 5 months. The NSOM results from these two years are presented in the Results and Discussion section and cover not only the planned activities but also include several new collaborations that were formed during this program.

Instrument Description

Near-field scanning optical microscopy (NSOM) has the potential to integrate optical and scanning probe microscopy (SPM) techniques and thus generate optical, electrical and structural images *with nanometer-scale resolution*. A state-of-the art NSOM-scanning probe microscope with unique UV capability (≥ 325 nm) has recently been established at Sandia. With this instrument, confocal microscopy (1000 nm resolution), near-field scanning, spectrally-resolved optical microscopy (≤100 nm resolution), and scanning-probe microscopy/atomic force spectroscopy (AFM, 5-100 nm resolution) experiments are performed concurrently (Figure 2).

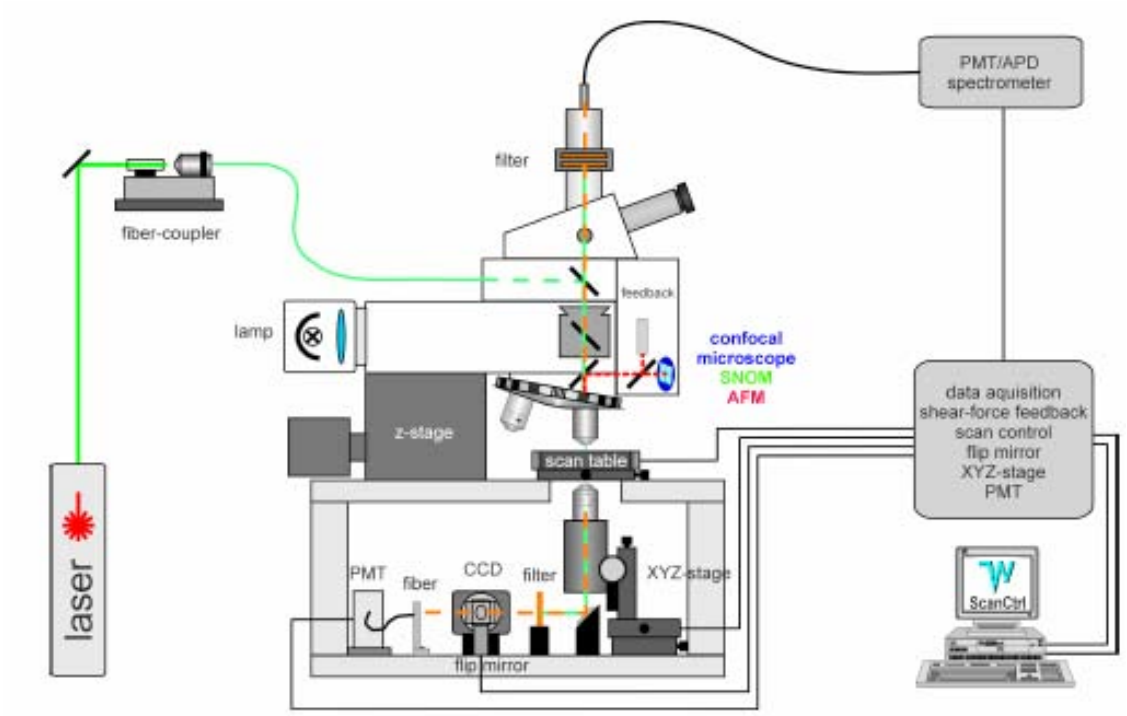

Fig. 2. Illustration of NSOM system.

Robust silicon/silicon nitride, aluminum-coated AFM cantilevers, with holes (80-100 nm in diameter) fabricated through the cantilever tip, are used as the apertures. This tip design extends the apertures scanning lifetime inhomogeneities compared a pulled optical fiber. With the NSOM instrument configured as shown in Fig. 2, surfaces can be imaged in an illumination mode (excitation through the aperture above the sample surface with detection below the sample), in a collection mode (excitation below the sample surface and detection through the aperture above the sample surface), and in an illumination/collection mode (excitation and detection through the aperture above the sample surface). The light sources used for the optical excitation are a single-mode fiber-coupled 325 nm HeCd laser and a 532 nm doubled YAG laser. The instrument is equipped with both a photomultiplier tube and an avalanche photodiode detector. For spectrally resolved light detection, a three turret (300 blaze 300 nm, 300 blaze 500 nm, 1800 blaze 300 nm gratings) spectrometer with thermo-electrically cooled UV-enhanced CCD (1064 x 256 2D array) camera is also fiber-coupled.

Near-field scanning optical microscopy achieves resolution higher than the diffraction limit by positioning the sample and the aperture defined light source into the near-field region such that the distance between the sample and tip is less than the wavelength of incident light as shown in Fig. 3. The area of sample illumination is determined by the size of the aperture and not the wavelength of light. An image is formed by moving the light source and sample relative to each other. While this idea was first proposed by E. H. Synge in 1928[6], it was not until the creation of bright sub-wavelength-sized light sources and the development of reliable feedback methods for control of holding an aperture in close proximity to a sample surface that NSOM was realized.

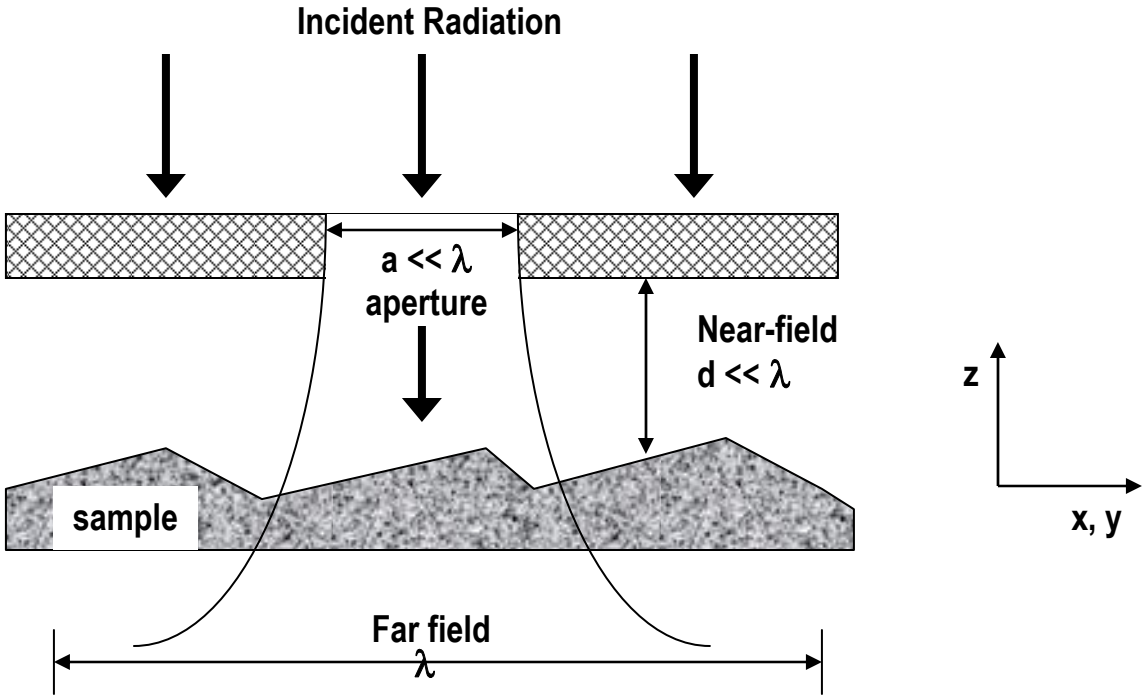

NSOM: E. H. Synge, Philos. Mag. 6 (1928) 356.
Cartoon: J. W. P. Hsu, Mater. Sci. Eng. 33 (2001) 1.

Fig. 3. An illustration of near-field operation of an NSOM is shown. The sub-wavelength aperture is placed in the near-field region (sub-wavelength distance) of the sample.

Results and Discussion

Cantilever Epitaxy of Gallium Nitride

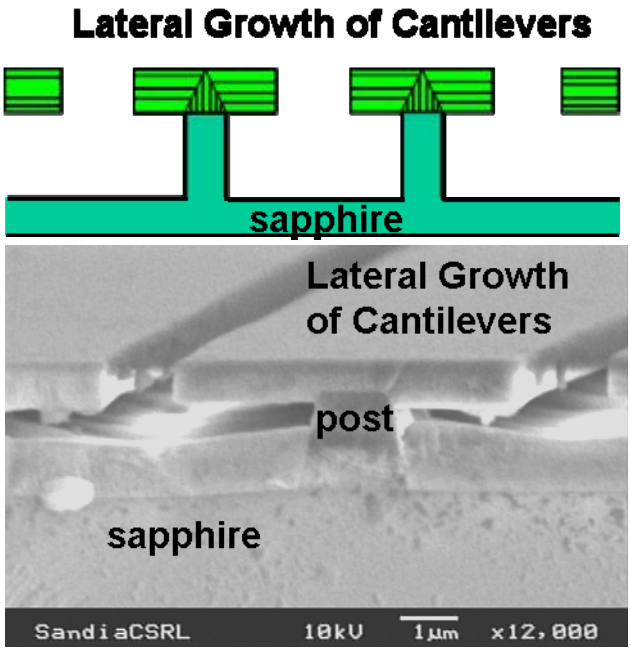

Fig. 4. Illustration and SEM image of Cantilever Epitaxy showing sapphire post, GaN pyramid, GaN lateral growth wings, and coalescence region.

Cantilever Epitaxy is an MOCVD growth method invented at Sandia that produces GaN with low dislocation densities by patterning lines on the sapphire growth substrate.[7,8] After deposition and annealing of a thin GaN nucleation layer and deposition of a thin GaN layer at 1050°C, the GaN growth temperature is decreased to 950°C to produce pyramidal facets (112-2) on top of the sapphire line. After the pyramidal facets are well formed, the GaN, as shown in Fig. 4 growth temperature is increased to 1080°C to promote lateral growth and coalescence of the GaN. As a result of the lateral growth the dislocations are turned above the posts to form uniform low dislocation-density GaN (2-3 x 10^7/cm^2).

The advantage of CE over epitaxial lateral overgrowth (ELOG) is that CE growth can be accomplished in a single MOCVD growth run. In contrast for ELOG growth, a dielectric material is deposited on previously grown GaN and a second GaN growth step is performed on the dielectric material, thus two growth steps are required for the ELOG dislocation reduction technique.

Confocal images were obtained of a not fully-coalesced CE sample are shown in Fig. 5. Higher GaN emission PL intensity is observed in the wing regions, corresponding to lower dislocation densities in that area of material. Lower PL intensities were observed over the sapphire post/line regions and the coalescence front regions, indicating areas of higher dislocation densities. Cathodoluminescence and AFM data support these correlations.[7]

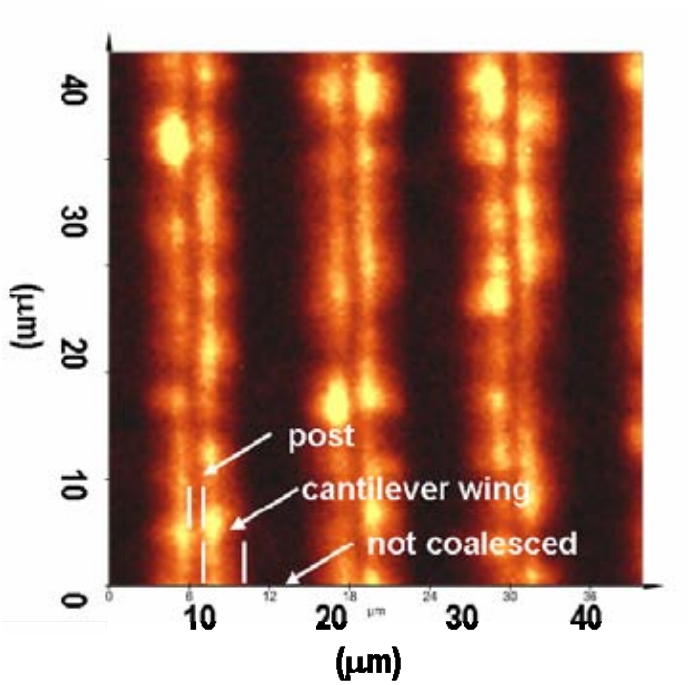

Fig. 5. Confocal image of PL from not fully-coalesced CE GaN sample showing differences in PL intensity as a function of post, wing, and coalescence-front structures, corresponding to lower (more PL intensity) or higher (less PL intensity) dislocation densities, respectively.

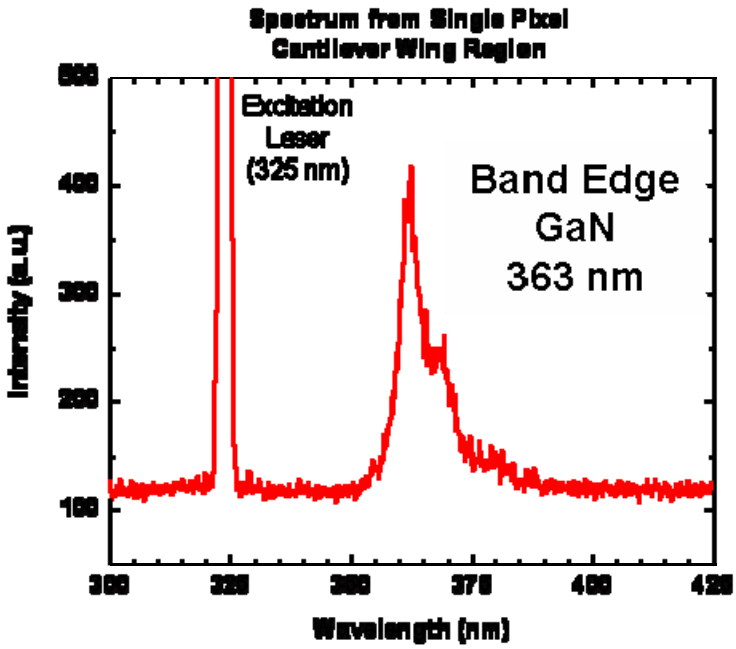

Fig. 6. Spectrally-resolved PL of GaN band edge emission from CE wing region (see Fig. 5).

The detected PL was spectrally-resolved by the spectrophotometer and an example spectrum is shown in Figure 6. The band-edge emission from GaN is expected to be at 363 nm and this peak position is observed in the sample. The shoulders to the band-edge peak likely correspond to lower quality GaN present in the trenches below the wings. Also seen in the spectrum is the reflected excitation laser light at 325 nm. The intensity of this reflection was useful in differentiating the positions of the post/line-wing region and the non-coalesced region, thus providing spatial identification for each of these regions.

Solar Cells

Electrical scanning probe techniques were implemented on the NSOM system for the solar cell analyses. A cadmium-telluride (CdTe) solar cell was cross sectioned with the goal to identify the position of the junction. The scanning probe method used was photovoltage. Substantial time was devoted to configuring the experiments to accommodate a large tip-surface impedance. Initial scanning-probe experiments were performed to map the band-bending of a CdTe solar cell cross-section. Consistent with the cell design, the width at open-circuit of the depletion region was comparable to our resolution (~0.1 μm), and the potential image consisted of a sharp step (Figure 7).

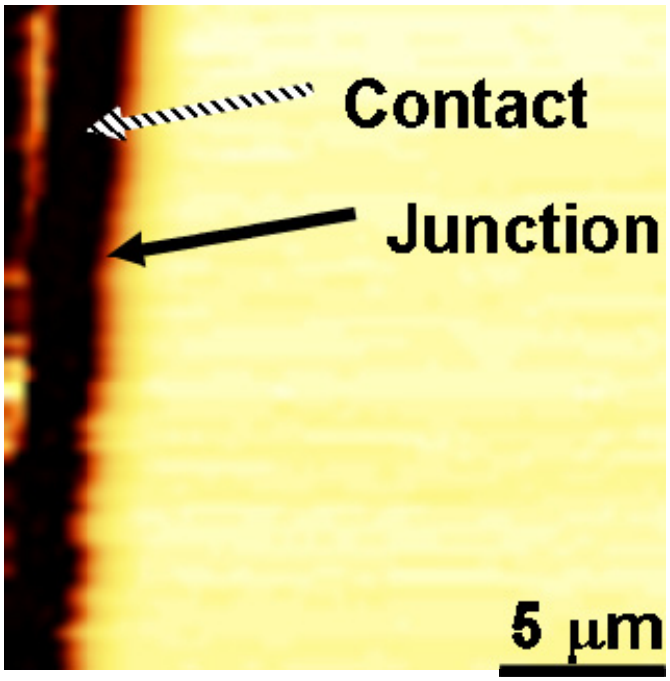

Fig. 7. Photovoltage scanning probe image of a cross section of a CdTe solar cell. The intensity corresponds to the potential/voltage as the sample was illuminated. The sharp step indicated the interface between the junction and the contact.

From out studies we concluded that the junction is too close to the metal contact to be resolved with a standard AFM tip (resolution ~25 nm). Also, sample preparation issues arose in that the metal contact on the solar cell appeared to be smeared into the junction region during the cross-sectional cutting procedure. Experiments to optimize sample

preparation and limit structural damage to the solar cells were discussed with the Metallurgy Laboratory, but the solar cell part of this LDRD was halted due to reallocation of Center 6000 resources.

Photoluminescence of Materials for InGaN and Green LEDs

Several SSL methods have been proposed for producing white light, including combinations of red, green, and blue (RGB) LEDs and combining blue or UV LEDs with down-conversion phosphors. The most efficient SSL white LEDs should be combinations of efficient RGB LEDs. Of the RGB LEDs, the least energy efficient LEDs are InGaN-based green LEDs. Green GaN-based LEDs require alloying with ~ 20% indium to produce wavelengths around 525 nm. Incorporation of >15% In leads to compositional fluctuations (clusters of In metal), v-defects around threading dislocation cores, and possibly point defects in the InGaN crystal lattice due to the low growth temperature necessary to incorporate the indium. These effects can decrease internal quantum efficiency by affecting carrier transport, carrier recombination, and light propagation. We investigated several aspects of InGaN materials and defect-related emission in InGaN quantum wells and LEDs.

Using confocal-mode microscopy, we compared LED emission, p-n junction photocurrent, and surface morphology for a Sandia-grown multi-quantum well (MQW) InGaN LED. Light emission, photocurrent, and surface morphology were obtained concurrently and all displayed the same features (Figure 8). Surface morphology was measured in the confocal mode by monitoring the reflected excitation laser light from the sample surface. We observed that light output (photocurrent) was enhanced by scattering off of large surface features such as hillocks and v-defects (morphology dark areas).

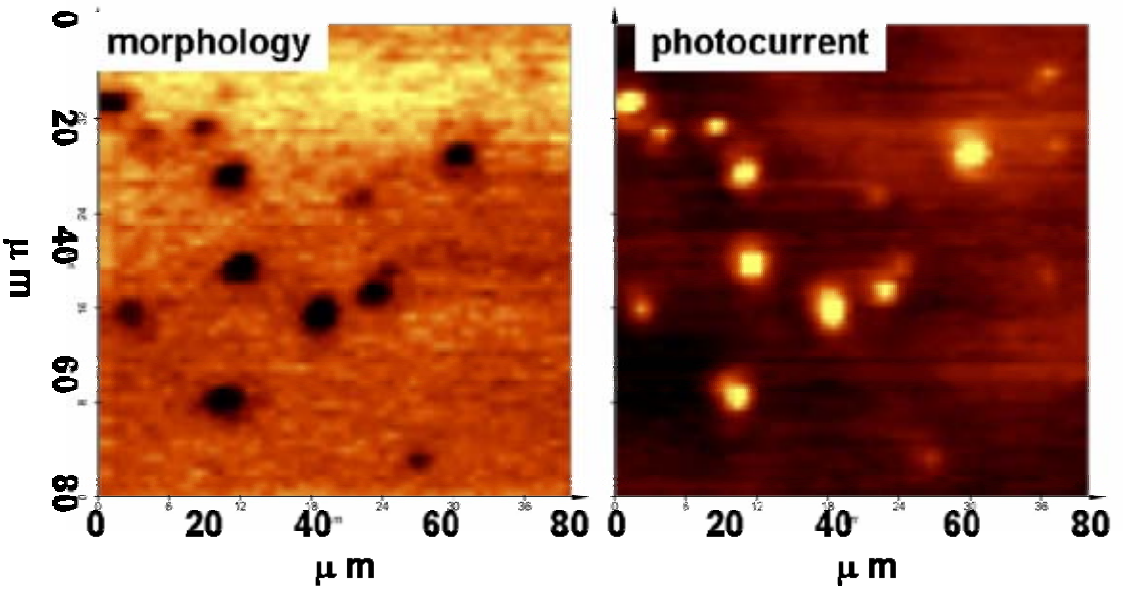

Fig. 8. Two-dimentional images of morphology and photocurrent from collected concurrently from a MQW InGaN LED correlating enhanced light output with large surface features.

The topic of indium segregation in InGaN alloys is hotly debated in the literature. Previous studies of InGaN alloys by NSOM report widely varying results, as discussed in the Introduction. In general, these studies agree that PL intensity and wavelength can vary in InGaN alloys, but none definitively observed In segregation and none were accompanied by further studies, such as a material matrix to determine the factors controlling phase separation, dislocation density, and effects on device operation.

Confocal imaging of an InGaN single quantum well (Emcore/Veeco) with our NSOM system indicated several aspects of wavelength-dependent PL, despite the low spatial resolution of confocal mode (~1 μm). An example image is shown in Fig. 9.

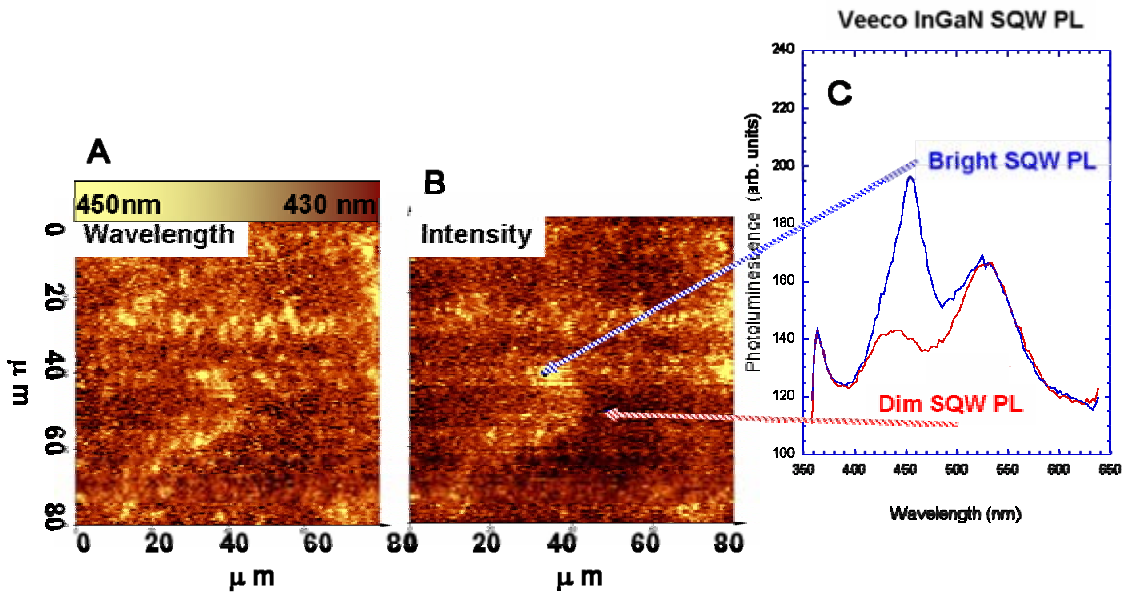

Fig. 9. 9a) 2-dimensional image of InGaN SQW indicating spatial variations in PL wavelength between 430 and 450 nm, 9b) concurrent 2-dimensional image of InGaN SQW indicating spatial variations in PL intensity, 9c) spectrally-resolved PL intensities as a function of wavelength obtained at the positions noted by the arrows showing SQW band-edge peak shifted by 15-20 nm to longer wavelength.

A 2-dimensional image of the InGaN SQW is shown in Figure 9a, indicating spatial variations in PL wavelength between 430 (yellow) and 450 nm (brown). Approximately 50% of emission between 420-470 nm originates from the bright yellow regions. Emission between 450-480 nm , the GaN "yellow-band" was more uniformly observed across the wafer. A concurrent 2-dimensional image of InGaN SQW indicating spatial variations in PL intensity (high intensity is yellow, low intensity is brown) is shown in Figure 9b. Spectrally-resolved PL intensities as a function of wavelength (Figure 9c) were obtained. At the position noted by the blue arrow, the bright-intensity region has a large component of PL emission at ~450 nm. At the position noted by the red arrow, the low-intensity region has a much smaller component of PL emission at ~430 nm. The SQW band-edge peak is shifted by 15-20 nm to longer wavelength in the bright-intensity regions. The magnitude of this wavelength shift corresponds to a 1-2% higher In content

in the bright-intensity regions of the material, suggesting possible indium segregation is present in these films.

In order to further investigate this phenomena, single and multiple InGaN quantum well samples were grown with varying In concentrations by varying the growth temperature. InGaN MQW samples with 5 wells were grown with 15.0 and 18.4 % indium content in the MQWs. The quantum well thicknesses were 27A and 31A, respectively, and the barrier thicknesses were 110A and 109A, respectively. A morphology survey using a Nomarsky optical microscope detected the presence of large ridge-like features on the sample surfaces Fig. 10, which are due to the delayed recovery growth mode used to reduce the dislocation density. AFM analysis (not shown) indicated the ridge features pushed out from the sample surface.

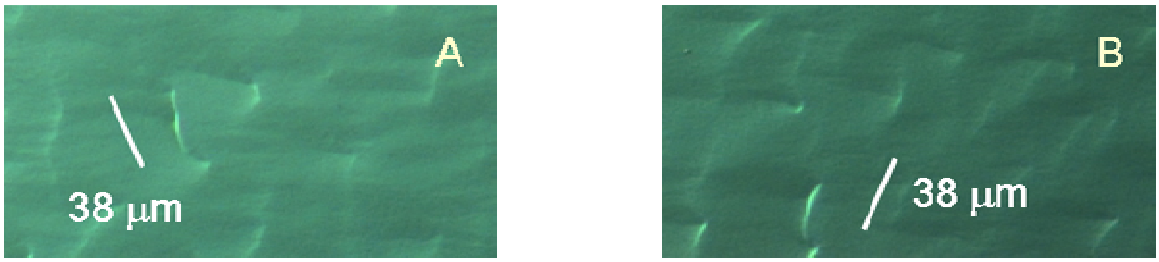

Fig. 10. Nomarksy optical images of 10a) 15.0% In 5 MQW, and 10b) 18.4% In 5 MQW surfaces showing presence of large ridge-like structures.

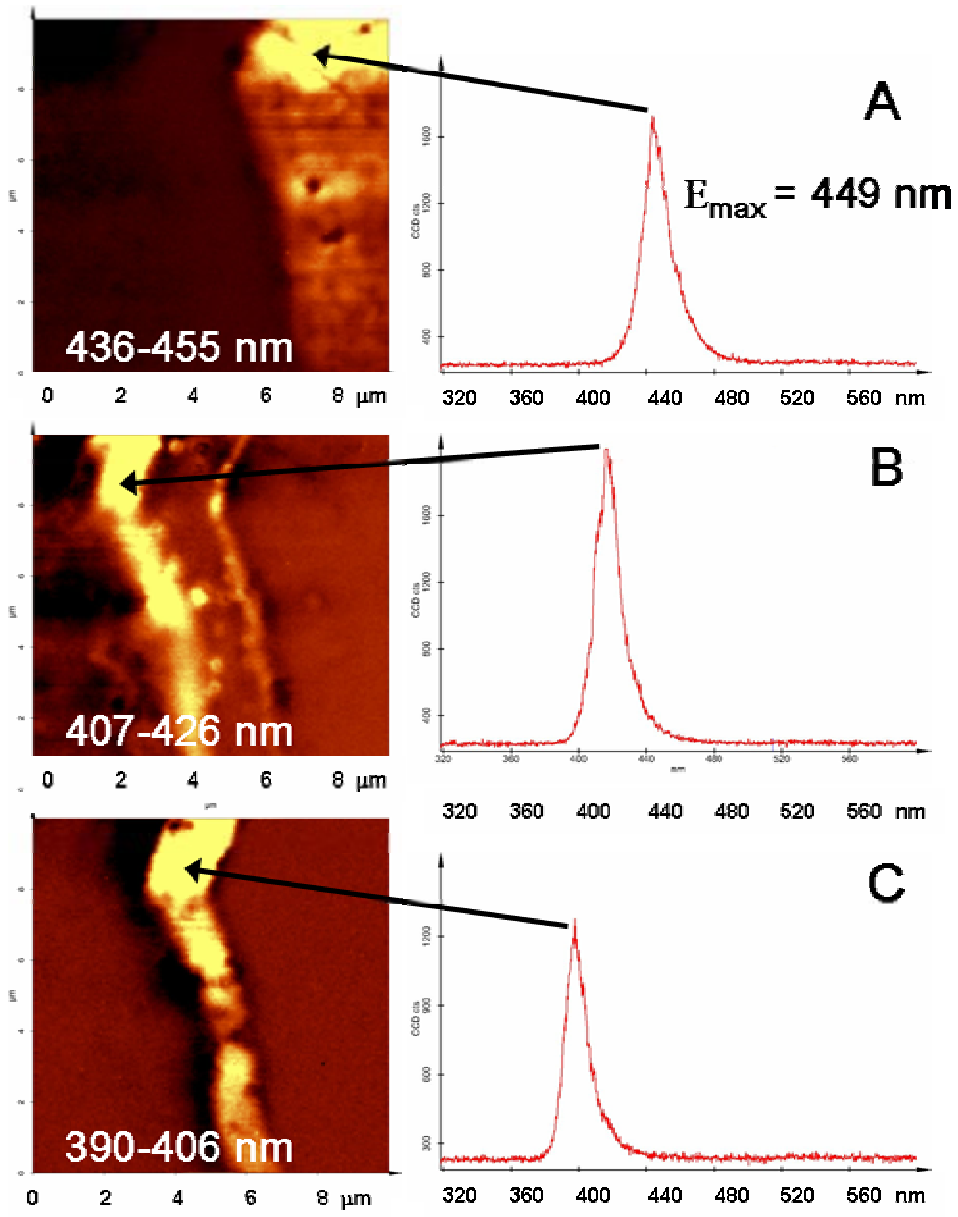

Fig. 11. Spatially-resolved 2-dimensional images of PL intensity between 436-455 nm (11a), 407-426 nm (11b), and 390-406 nm (11c), collected as the NSOM tip scanned over the ridge feature. Spectrally-resolved data for PL intensity as a function of wavelength corresponding to the locations of the arrows are also presented for 11a, 11b, and 11c, and indicate that the emission wavelength blue-shifts from the expected emission maximum (449 nm) by up to 65 nm across the ridge feature.

Two-dimensional, spectrally-resolved images in NSOM collection mode were obtained for both of these samples using a ~100 nm aperture, collecting 128 pixels/10 µm and 16384 spectra/image. Data for the 15.0% In sample are shown in Fig. 11. Spatially-resolved 2-dimensional images of PL intensity are shown in Figure 11 for three wavelength regions, 436-455 nm (11a), 407-426 nm (11b), and 390-406 nm (11c). The

images were collected as the NSOM tip scanned over the ridge feature. Spectrally-resolved data for PL intensity as a function of wavelength were also obtained. Shown in Figure 11 are the spectra corresponding to the locations of the arrows for 11a, 11b, and 11c. These data indicate that the emission wavelength blue-shifts from the expected emission maximum (449 nm) by up to 65 nm over the ridge feature.

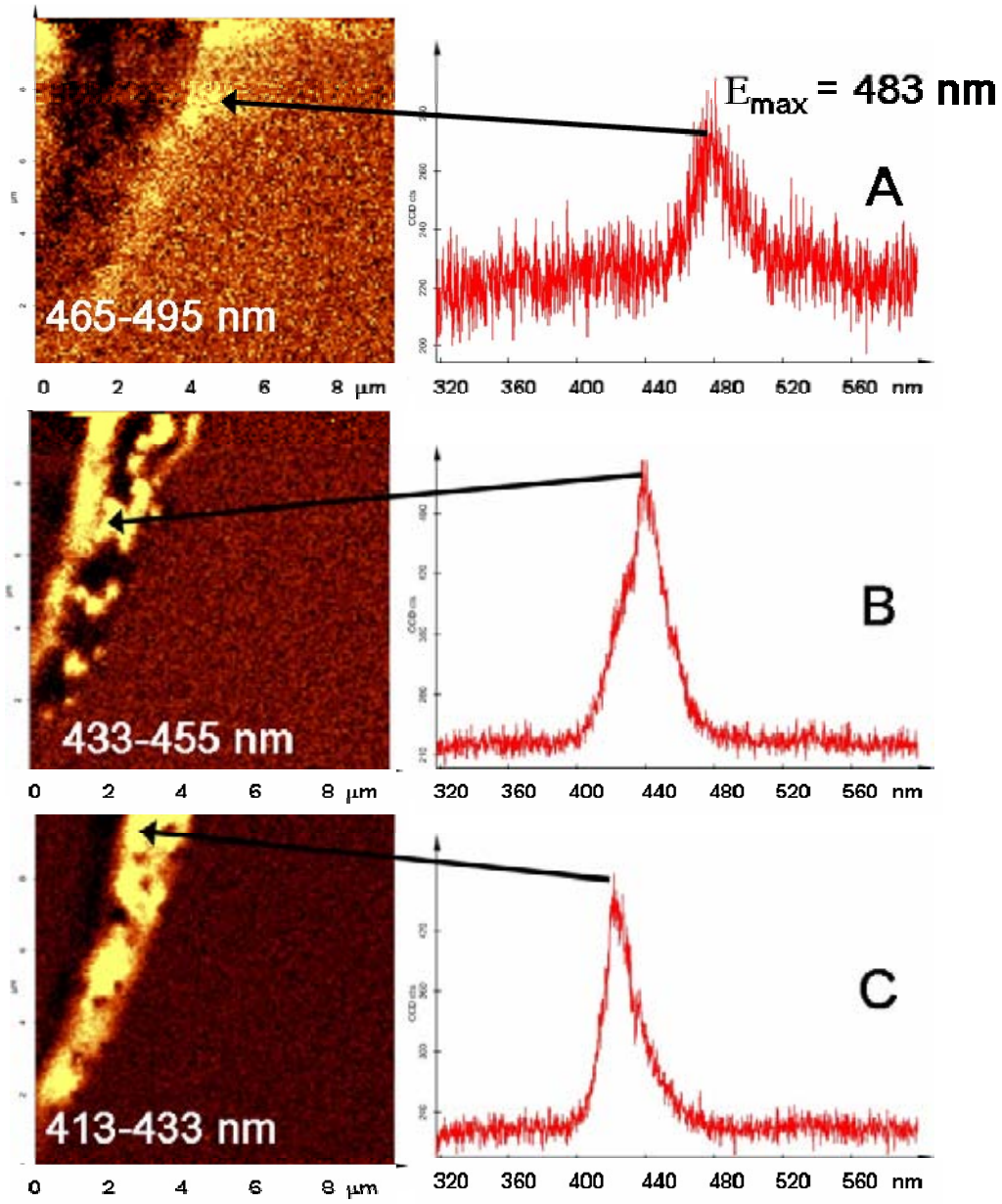

Fig. 12. Spatially-resolved 2-dimensional images of PL intensity between 465-495 nm (12a), 433-455 nm (12b), and 413-433 nm (12c), collected as the NSOM tip scanned over the ridge feature. Spectrally-resolved data for PL intensity as a function of wavelength corresponding to the locations of the arrows are also presented for 12a, 12b, and 12c, and indicate that the emission wavelength blue-shifts from the expected emission maximum (483 nm) by up to 82 nm across the ridge feature.

Similar data was observed for the 18.4% In MQW samples (Fig. 12). With the higher In content (18.4%), the expected wavelength for maximum emission is 483 nm. We observed a blue-shift in the PL wavelength of 82 nm over the ridge features in this sample. We postulate this wavelength shift is due to decreased QW thickness and/or reduced indium incorporation over the ridge feature. Thinner quantum wells with reduced indium content will cause an increase the bandgap, shifting the PL emission to shorter wavelengths as experimentally observed in Figs. 11 and 12.

NSOM Collaborations within Sandia National Laboratories

As noted above, expanding awareness of our new NSOM-based capabilities at Sandia was an important milestone for this unique Junior/Senior Mentor LDRD. We were able to form several new collaborations with our Sandia colleagues and Sandia-funded projects as well as with the NINE University partners on these projects. Below we will describe the collaborative project and discuss some of our NSOM-based results.

Nanoscience Studies of InGaN Materials and LEDS for Improved IQE with M. H. Crawford, S. R. Lee, A. J. Fischer (1123), D. K. Koleske (1126), N. A. Missert, 1112, E. Fred Schubert, Shawn Lin, Christian Wetzel (Rennselaer Polytechnic Institute), Late Start LDRD FY06.

This project is the study of nanoscale InGaN materials properties to fundamentally improve internal quantum efficiency of light emitting materials, especially at deep green wavelengths (540-550 nm) where the emission efficiency decreases dramatically. To achieve the higher indium contents for green light emission lower growth temperatures are required. At these lower growth temperatures the InGaN/GaN MQW growth induces v-type inverted pyramidal defects that contain inclined facets (11-01) with the pyramidal apex located on a threading dislocation. InGaN quantum wells and barriers grown over these inclined facets result in are thinner than the QW and barrier thicknesses on the (0001) plane, resulting in reduced quantum confinement and lower emission efficiency[9] For part of this project we have studied InGaN QWs grown on low-temperature GaN or InGaN underlayers to control the extent of the v-defects and the samples have been examined by advanced nanoscale materials characterization techniques (AFM, NSOM, cathodoluminescence (CL), X-ray diffraction).

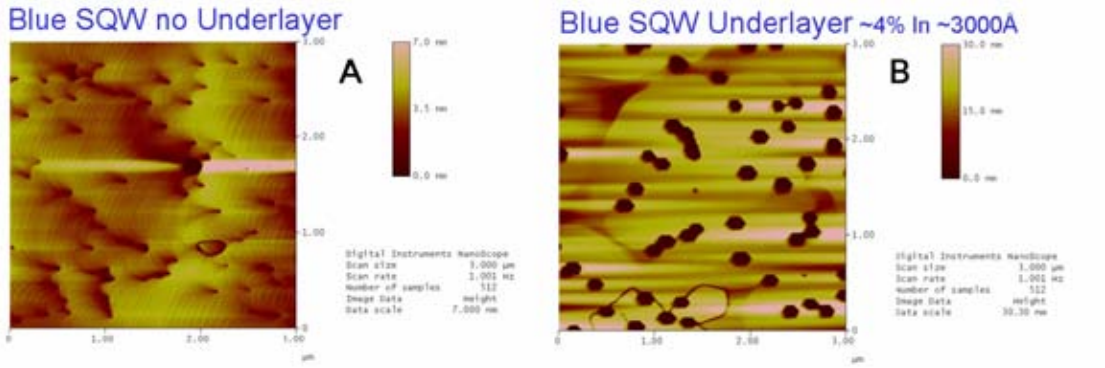

Fig. 13. AFM tapping mode images of InGaN SQWs without (13a) and with (13b) InGaN underlayers.

AFM images taken for two InGaN SQW structures shows the effect of an InGaN (~4% In, ~3000A thick) underlayer on v-defect formation (Fig. 13). The InGaN SQW surface grown without an underlayer (Figure 13a) has small v-defects (< 50 nm) that tend to pin the step-flow growth regions of the InGaN. In contrast, the InGaN SQW surface grown over a 4% InGaN underlayer has large (~185 nm), hexagonally-shaped v-defects. PL emission from the sample with the InGaN underlayer is ~10x brighter than the sample with no underlayer. Studies are currently underway to determine if the increase in brightness is due to improve internal quantum efficiency or if pyramidal facets increased light extraction.

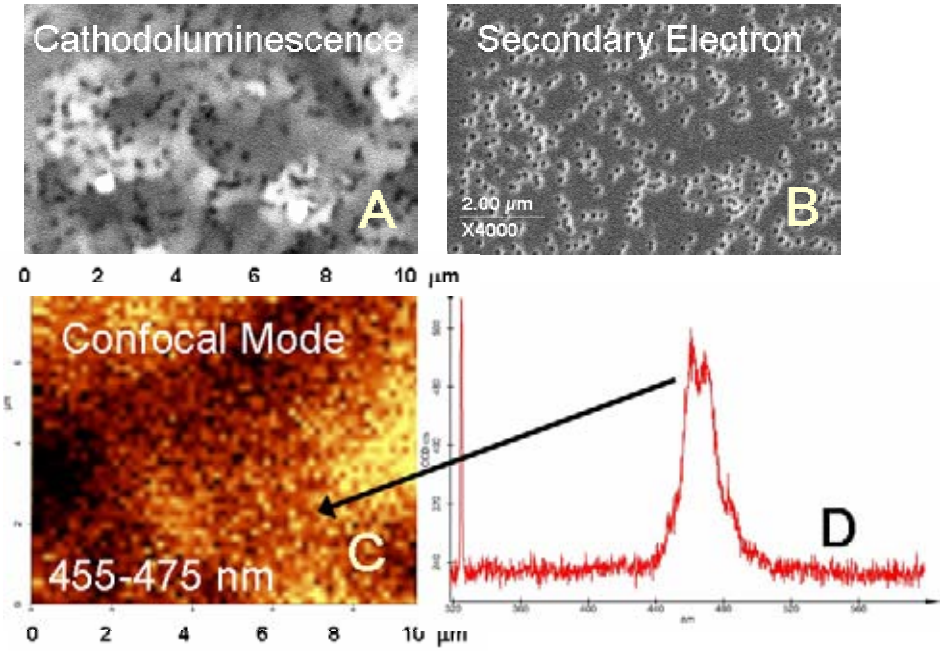

Fig. 14. Comparative luminescence images of InGaN 5MQW sample grown on a 2% InGaN underlayer 14a) cathodoluminescence, 14b) concurrent secondary electron, 14c) NSOM confocal mode PL emission averaged over 455-475 nm, yellow areas correspond to brighter PL, and 14d) spectrum from area at arrow from confocal PL image (14c).

A comparison of confocal mode PL and CL for a 5 MQW sample grown on a 2% InGaN underlayer is shown in Figure 14. In Figure 14a, the CL shows areas of brighter luminescence intensity on the order of ~0.5 µm to 2 µm. The very dark areas of much smaller dimensions correspond to v-defects (see also the darker areas of Fig. 14b). Analysis of the same sample by confocal PL (resolution ~ 1 µm) shows brighter luminescent regions (yellow) over much larger dimensions than CL, on the order of several micrometers. NSOM mode PL acquisition at much higher resolution (~100 nm) with concurrent acquisition of AFM data is on-going.

We have been able to detect PL in NSOM transmission mode, where the excitation laser is going through the aperture above the wafer and PL is detected below the wafer. One issue is that most of the samples are grown on single-sided polished sapphire wafers,

thus the detected emission is scattered by the rough backside of the wafer and resolution may be lost. The ability of carriers to move in the sample prior to radiant recombination is another concern when detecting without using an aperture. The solutions to these concerns include using double-sided polished wafers or polishing the backside of single-sided polished wafers and performing the experiment in illumination/collection mode where excitation and detection are performed thorough the aperture. This method is difficult to achieve as the narrow cone of acceptance dictated by the aperture excludes the great majority of the emitted light.

Another issue that may affect resolution is, at an excitation wavelength of 325 nm, we are inducing PL in the GaN layers as well as the InGaN material. The GaN emits at ~363nm, and may induce PL in the InGaN materials. Incorporation of a different excitation laser at a longer wavelength (~400 nm) would address this issue by limiting PL excitation to resonant excitation of the InGaN quantum wells and not induce emission in the GaN underlayers. A GaN laser at 405 nm would achieve the resonant excitation and would deliver light at a much higher power than the 325 nm laser. The caveat here is that resonant excitation will only occur in the InGaN quantum wells, so the volume of material excited will be small, due to the thinness of the quantum wells *versus* a bulk film, and the resulting emission intensity may also be low.

GaN-based Nanowires with G. T. Wang (1126)

For this project MOCVD is used to grow GaN, AlGaN, AlN, and InGaN nanowires using solid/liquid/vapor catalyst method, using metals such as nickel for the catalysts. The nanowires can be grown with both n-type and p-type doping, and one goal is to grow a p-n junction structure within a single wire. The wires can be fabricated into diodes for electroluminescence (EL) studies in addition to more conventional PL studies.

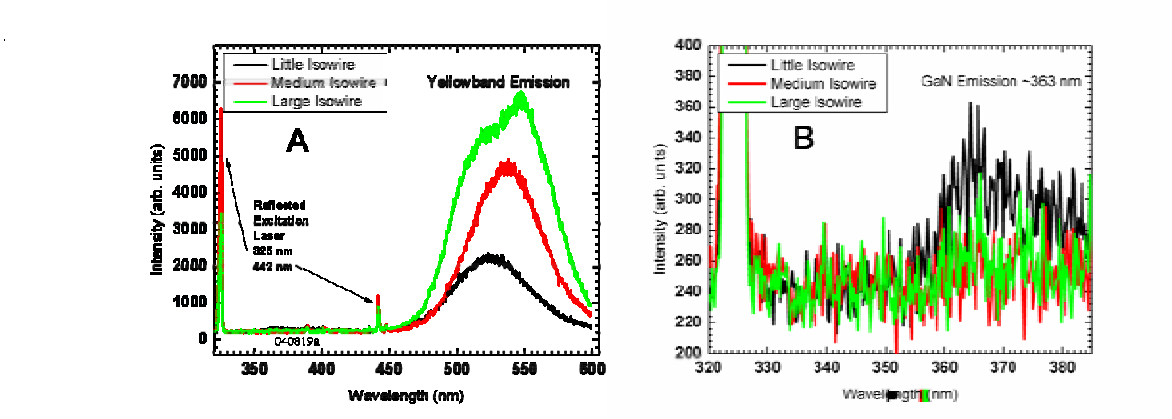

Fig. 15. Confocal NSOM PL of small, medium, and large isolated GaN nanowires (15a), and expanded region of bandedge emission at ~363 nm (15b).

We have used confocal mode of the NSOM system to excite PL in isolated GaN nanowires (Fig. 15). We generated PL from small, medium, and large isolated nanowires. Each wire size exhibited an intense, broad emission at ~540 nm, corresponding to GaN "yellowband" emission, which is believed due to defects in the GaN material (Fig. 15a).

Bandedge emission at ~363 nm was also observed, and an expanded bandedge region of the spectra is shown in Fig. 15b. Further studies will be performed on In and Al alloys of GaN and direct comparisons between PL and EL will be made.

Polymeric Materials for Organic Light Emitting Diodes with C. H. Fujimoto (6219)

The project is examining dichloromethane-based polymers for novel white light OLED-based applications. The polymers can be functionalized and spin-coated onto various substrates. Fabrication into diodes is also performed. We used conventional PL with 325 nm excitation and confocal PL to analyze the emission properties of these polymers. The conventional PL data are shown in Fig. 16.

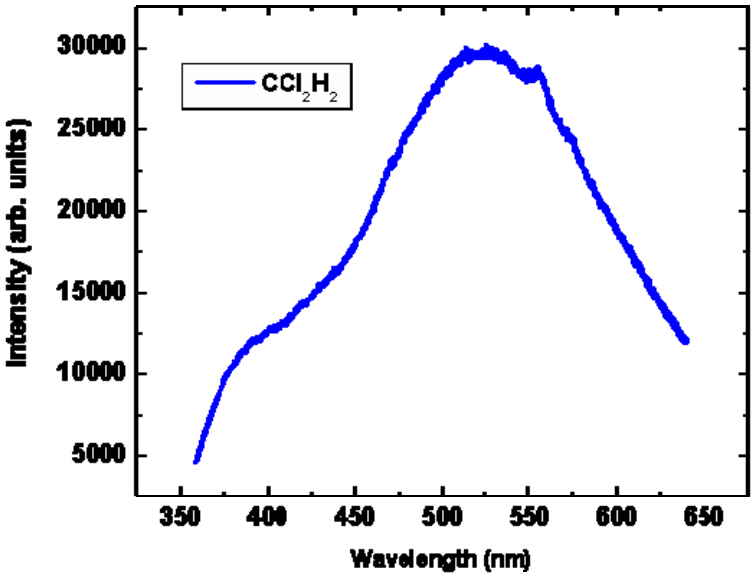

Fig. 16. Conventional PL of poly-dichloromethane spin-coated onto a glass substrate.

The PL is composed of a broad emission centered about 400-600 nm. There are possible 3-4 emission bands within the PL envelope. We observed some initial decrease in PL intensity with the initial laser excitation, but the PL intensity then stabilized with further exposure to the excitation laser. PL obtained from 5 locations across the substrate showed similar profiles and intensities, indicating good uniformity. Some of the detected emission is believed due to the glass substrate used, but the general wavelength band and reasonable intensity levels are due to the polymer.

Confocal PL was attempted with the NSOM system, but no PL was detected. We believe this is due to the much lower excitation power of the 325 nm NSOM source (~1.5 mW) as compared to the conventional 325 nm laser (100-1000 mW). Further collaborations will investigate other polymers using the NSOM system and OLED processing with these polymers at Sandia. This collaboration lead to successful proposal selection to the BES Hydrogen Fuel Initiative program.

<u>Phase Imprint Lithography for Large Area 3D Nanostructures</u> with G. R. Bogart (1747), F. B. McCormick, R. Ellis, D. W. Peters (1713-1), D. R. Wheeler(1743), J. W. P. Hsu (1114), R. K. Grubbs (2452), D. Noble (1513), and J. A. Rogers (University of Illinois Urbana-Champaign)

This project is a late start LDRD developing the capability to fabricate large areas of 3D nanostructures for applications including nanoporous filter elements for high surface area sensors and separators, high-efficiency catalyst supports, sub-wavelength optical filters, and surfaces to control wetting phenomena and facilitate drug delivery. The key element is a conformable, elastomeric phase mask with features of relief having dimensions comparable to optical wavelengths. The phase mask is placed on top of photoresist with atomic-level precision in the z-direction via van der Waals forces. Passing light through the mask generates a complex 3D distributing of intensities that expose certain regions of the photopolymer, generating photoacids that crosslink the photopolymer. The geometry of the distribution depends on the depth and layout of mask relief structures, mask refractive index, and the wavelength, coherence, and polarization of the exposure light. Unexposed areas are removed with suitable solvents. The 3D structures are thus formed with a single lithographic exposure (Figure 17).[10]

Fig. 17. Schematic cartoon of 3D structure fabrication with phase mask lithography and resultant 3D structure.

The structure shown in Figure 17 was fabricated at Sandia by successfully transferring the processing and expanding fabrication capabilities to utilize larger area conventional contact/proximity lithographic tools (Suss MA-6).

The elastomeric phase mask can be characterized with the NSOM system in "Pick-up Mode". In this application, the excitation light is brought in through the bottom of the phase mask and the complex light pattern generated by the interaction of the excitation light with the phase mask is detected through the NSOM aperture above the phase mask (Figure 18).

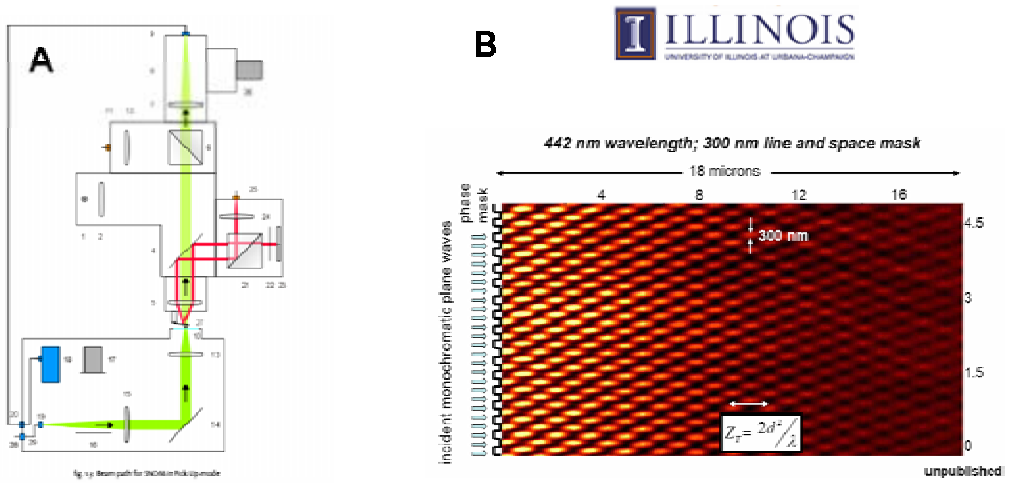

Fig. 18. Schematic of NSOM setup for Pick-up mode (18a) and resultant 2D image of 442 nm collimated laser light after interacting with the phase mask (18b).

We are in the process of setting up this capability in our NSOM system. We have determined that when using our 532 nm fiber-coupled laser source, we detect too much scattered laser light from around the NSOM cantilever aperture tip. The next step is to remove the fiber from the laser and incorporate a conventional, "table-top" optical train to steer and focus the laser into the NSOM system.

Summary

The goal of this LDRD was to improve our understanding of radiative and non-radiative mechanisms in material nanostructures through the combination of optical and scanning-probe microscopy methods for surface, materials, and device analyses to improve LED and solar cell efficiencies. We were able to utilize our new NSOM system to aid in understanding defect-related emission issues in GaN-based materials. We observed micrometer-scale variations in PL for GaN grown by Cantilever Epitaxy with lower emission intensity observed in regions of higher dislocation densities. Electrical capabilities were added to the NSOM system, allowing concurrent detection of photocurrent and surface morphology for InGaN MQW LEDs. From these studies blue-shifted emission with lower intensity were observed at hillock-shaped material defects. We identified evidence for possible indium segregation in InGaN quantum well materials by observing both emission intensity variations and wavelength shifts in spatially- and spectrally-resolved PL. We also detected a blue-shift in InGaN MQW emission that was due to thinning of quantum wells grown on top of large-scale (μm) v-defect structures in GaN. We also expanded the awareness of our new NSOM/multifunctional SPM capability at Sandia and formed several collaborations within Sandia and with NINE Universities. From these new collaborations several studies of on GaN-based compound semiconductors for green LEDs, nanoscale materials and nanostructures, novel application of polymers for OLEDs, and phase imprint lithography for large area 3D nanostructures were investigated.

References

[1] M. S. Jeong, Y.-W. Kim, and J. O. White, Applied Physics Letters **79**, 3440 (2001); Crowell, Applied Physics Letters **72**, 927 (1998); Young, Applied Physics Letters **74**, 2349 (1999); Kaneta, Applied Physics Letters **81**, 4353 (2002).

[2] Vertikov, Applied Physics Letters **72**, 2645 (1998).

[3] M. S. Jeong, Applied Physics Letters **79**, 976 (2001).

[4] Vertikov, Applied Physics Letters **73**, 493 (1998).

[5] Kim, Applied Physics Letters **80**, 989 (2002).

[6] E. H. Synge, **6**, 356 (1928).

[7] C. C. Mitchell, Master of Science, University of New Mexico, 2003.

[8] C. I. H. Ashby, C. C. Mitchell, J. Han et al., Applied Physics Letters **77**, 3233 (2000).

[9] Hangleiter, Physics Review Letters **95**, 127402 (2005).

[10] S. Jeon, J.-U. Park, S. Yang et al., Proceedings of the National Academy of Sciences **101**, 12428 (2004).

Distribution

1	MS0123	LDRD Office, 01011
1	MS0888	C. H. Fujimoto, 06338
1	MS1033	M. A. Quintana, 06337
1	MS1080	G. R. Bogart, 01747
3	MS1086	K. H. Bogart, 01126
1	MS1086	R. M. Biefeld, 01126
1	MS1086	Department Files, 01126
1	MS1086	M. H. Crawford, 01123
1	MS1086	D. D. Koleske, 01126
1	MS1086	G. T. Wang, 01126
1	MS1104	R. D. Robinett, 06330
1	MS1110	J. S. Nelson, 06337
2	MS0899	Technical Library, 04536
2	MS9018	Central Technical Files, 08944